

Investigation of the groundwater system at Masaya Caldera, Nicaragua, using transient electromagnetics and numerical simulation

Richard E. MacNeil^a, Ward E. Sanford^{b,*}, Charles B. Connor^a,
Stewart K. Sandberg^a, Mikel Diez^a

^a Department of Geology, University of South Florida, 4202 East Fowler Avenue, SCA 528, Tampa, FL 33620, USA

^b United States Geological Survey, mail stop 431, Reston Va. 20192, USA

Received 24 January 2007; accepted 31 July 2007
Available online 14 August 2007

Abstract

The distribution of groundwater beneath Masaya Volcano, in Nicaragua, and its surrounding caldera was characterized using the transient electromagnetic method (TEM). Multiple soundings were conducted at 30 sites. Models of the TEM data consistently indicate a resistive layer that is underlain by one or more conductive layers. These two layers represent the unsaturated and saturated zones, respectively, with the boundary between them indicating the water-table elevation. A map of the TEM data shows that the water table in the caldera is a subdued replica of the topography, with higher elevations beneath the edifice in the south-central caldera and lower elevations in the eastern caldera, coinciding with the elevation of Laguna de Masaya. These TEM data, combined with regional hydrologic data, indicate that the caldera is hydrologically isolated from the surrounding region, with as much as 60 m of difference in elevation of the groundwater table across caldera-bounding faults. The water-table information and estimates of fluxes of water through the system were used to constrain a numerical simulation of groundwater flow. The simulation results indicate that basalt flows in the outer parts of the caldera have a relatively high transmissivity, whereas the central edifice has a substantially lower transmissivity. A layer of relatively high transmissivity must be present at depth within the edifice in order to deliver the observed flux of water and steam to the active vent. This hydrologic information about the caldera provides a baseline for assessing the response of this isolated groundwater system to future changes in magmatic activity.

© 2007 Published by Elsevier B.V.

Keywords: caldera; groundwater; electromagnetic methods; geothermal evaluation; hydrology; volcanic structure

1. Introduction

Volcanic eruptions occur when magma exsolves sufficient volatiles to accelerate flow by rapid volume expansion, typically in the upper few kilometers of the crust. As the magma ascends through the crust it may interact with shallow groundwater in several ways. First, degassing of volatiles from the magma may create a

pressure gradient that can actually drive groundwater to the surface (Delaney, 1982; Newhall et al., 2001). Sudden onsets of spring discharge have been observed during the initial stages of several volcanic eruptions, such as the eruption of Mt. Pinatubo, Philippines; Usu volcano, Japan; and the Soufriere Hills volcano, Montserrat (Newhall et al., 2001; Shibata and Akita, 2001; Sparks, 2003). Second, magma can heat groundwater directly, sometimes resulting in phreatic eruptions. Such phreatic eruptions often herald the onset of episodes of volcanic eruption before magma reaches the surface, as was the

* Corresponding author.

E-mail address: wsanford@usgs.gov (W.E. Sanford).

case at Cerro Negro volcano, Nicaragua, in 1995 (Connor et al., 1996). Transient boiling of groundwater may continue for millennia when magma exists in buoyant equilibrium in the shallow crust, creating shallow hydrothermal systems (e.g., Hayba and Ingebritsen, 1997; Goff and Janik, 2000; Ingebritsen et al., 2006). Finally, direct interaction between groundwater and magma, particularly in confined aquifers, may initiate a fuel-coolant reaction that results in extremely violent phreatomagmatic eruptions (Morrissey et al., 2000). Thus, knowledge of the interaction between groundwater and

shallow magmatic systems can be crucial to understanding eruptions and the nature of heat and mass transfer in volcanic systems.

Nevertheless, the distribution and flow of groundwater is poorly known for the vast majority of active volcanoes (Hurwitz et al., 2003), and hydrologic properties of active volcanoes are rarely characterized. This situation persists because such volcanic systems are not typically developed for their groundwater resources. The fact that these systems need to be characterized with scant or nonexistent borehole access

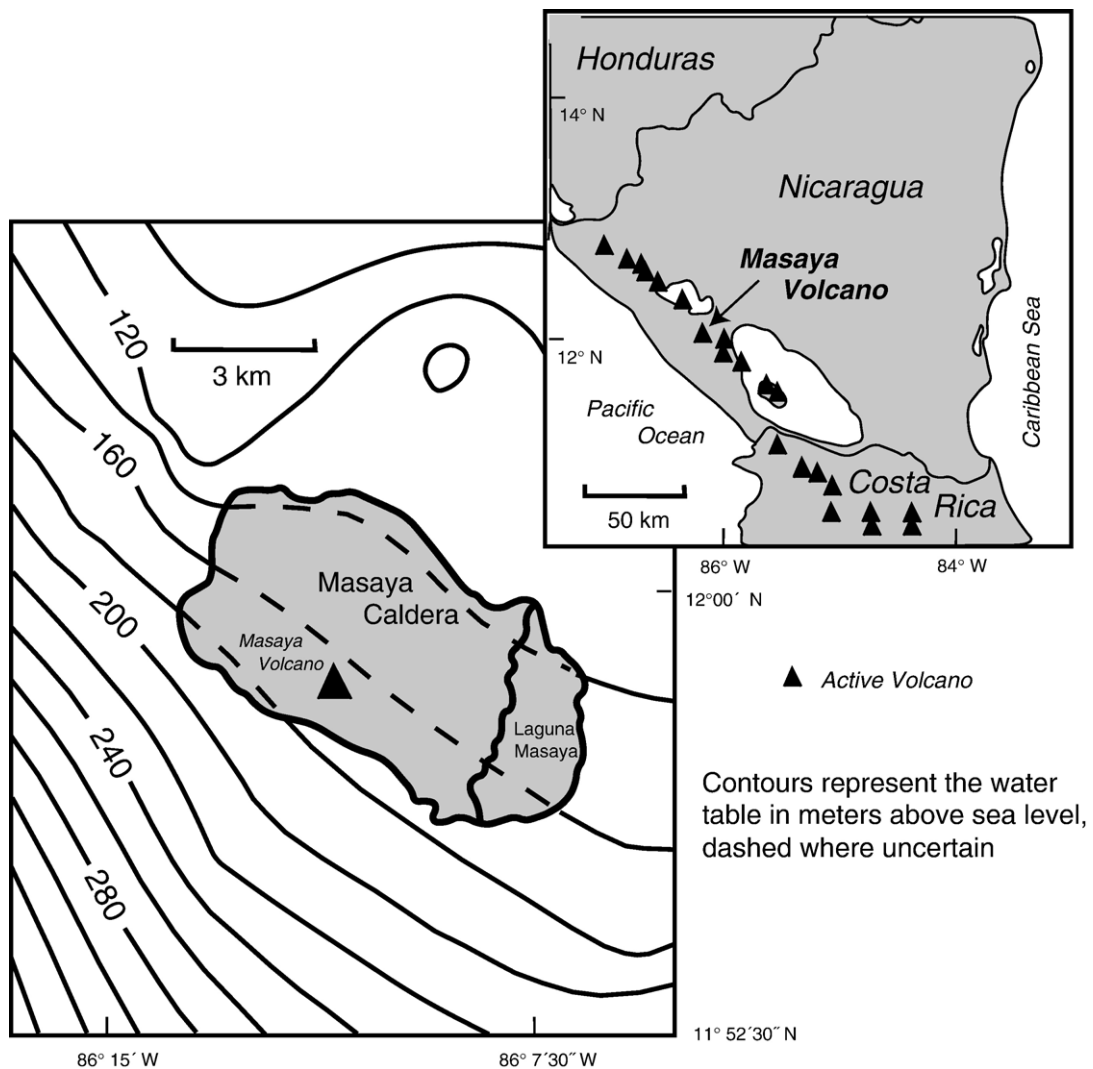


Fig. 1. Outline of Masaya caldera rim with regional groundwater contours. Contours are interpolated across caldera based on water level data in wells and from a regional ground water flow model developed by the Instituto Nicaraguense de Acueductos y Alcantarillados (INECAR) and the Japanese International Cooperation Agency (JICA). Regional groundwater level varies from ~190 m above sea level south of the caldera to ~130m above sea level north of the caldera (ENECAL and JICA; 1993). Inset shows location of Masaya volcano along a portion of the Central American volcanic arc in Nicaragua within the Nicaragua Depression, a NW-trending fault zone resulting from oblique subduction of the Nazca plate beneath the Caribbean plate.

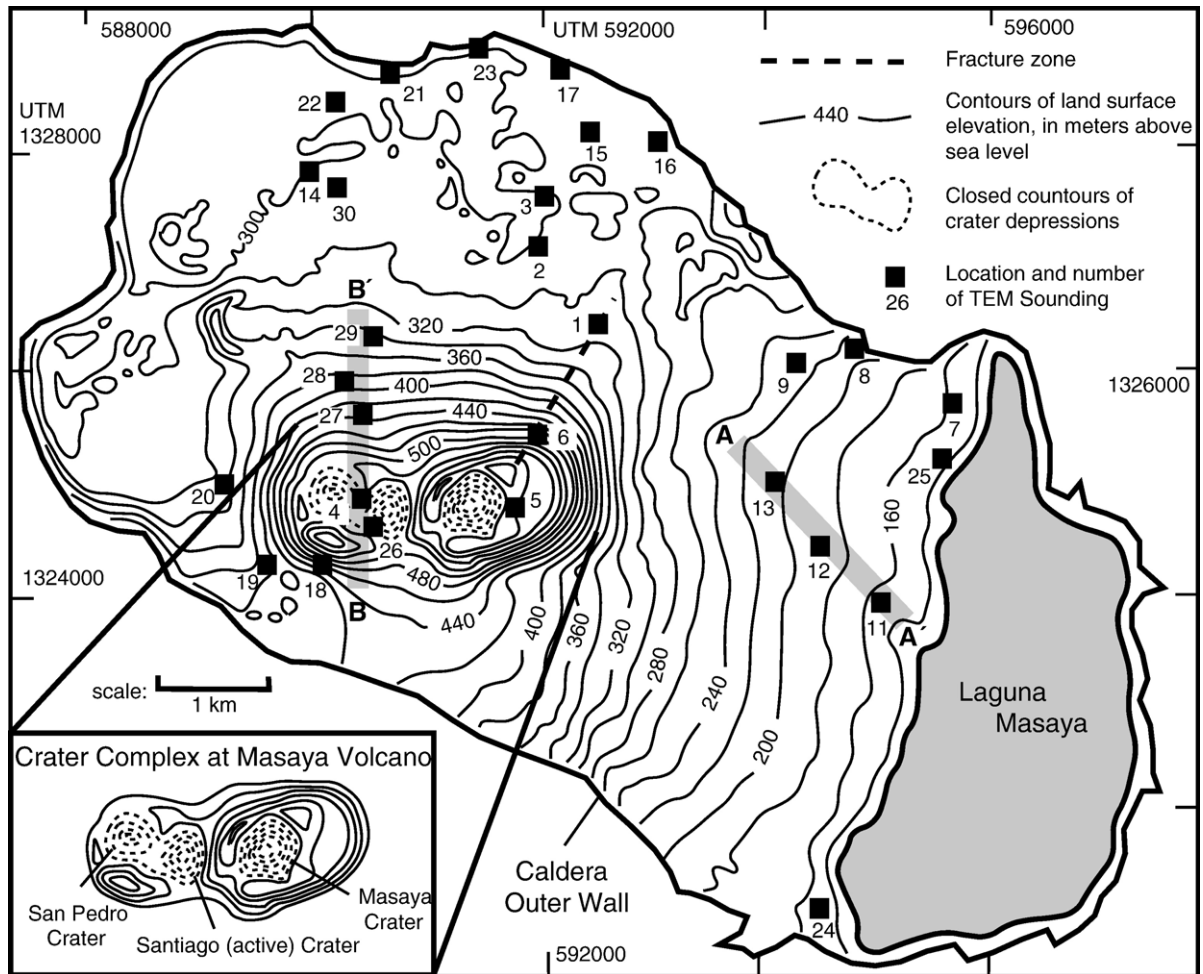


Fig. 2. Topographic map of Masaya caldera with locations of transient electromagnetic (TEM) soundings and profile lines. The caldera rim is inferred on the northern and southern sides. Inset shows details of the edifice and active crater region. The dashed line indicates the approximate trace of a fracture system on the NE Flank of Masaya volcano. Low temperature fumaroles occur in the area of TEM Station 1, along this fracture system.

suggests a need for remote sensing via geophysical methods such as transient electromagnetic (TEM) soundings along with innovative inversion techniques. The interpretation of resistivity in volcanic systems is complicated because the solutions are commonly non-unique (Kauahikaua, 1993 and Lénat et al., 2000). Resistivity in volcanic systems is affected by large temperature gradients, multi-phase flow, hyper-saline brines, and occurrences of clay-rich alteration minerals. Separating the effect of these variables in order to determine depth to the water table can be problematic.

Here, we employ TEM to constrain depth to the groundwater table at Masaya Caldera, Nicaragua, one of the largest active basaltic calderas on Earth (Fig. 1). At Masaya caldera, conditions for interpretation of resistivity soundings are less problematic than at some volcanic

systems, as there is generally an absence of saline water and clay alteration in the Holocene stratigraphic section, except for their probable existence in the hydrothermally active zone located near the active vent.

We present estimates of depth to the groundwater table within the caldera based on interpretation of 29 TEM soundings from 30 TEM sites. These data are compared with water levels measured in wells outside the caldera. Uncertainty in depth estimates is constrained by using alternative one-dimensional inversion methods. Our results suggest that Masaya caldera is isolated hydrologically from the surrounding regional groundwater flow system by its caldera-bounding faults and that the caldera's water table is a subdued reflection of the topography, except near the active Santiago vent, where dramatic gradients occur.

2. Masaya Caldera: a volcanic and hydrologic system

Masaya volcano, Nicaragua (11.98°N, 86.15°W) is part of the large complex of Pleistocene–Holocene shield volcanoes, nested calderas, small composite cones, cinder cones, and pit craters that are collectively referred to as Masaya caldera (Fig. 1). This complex is part of the Central America volcanic arc, which is characterized during the Quaternary by predominantly basaltic volcanic systems formed within and along the Nicaragua Depression, a NW-trending fault zone that accommodates dextral slip resulting from oblique subduction (DeMets, 2001; La Femina et al., 2002). Volcanoes and faults associated with the arc and Nicaragua Depression are the dominant structures near Masaya caldera.

This volcano complex has been the site of tremendous Plinian basaltic eruptions during the last ~6 ka (Williams, 1983a; van Wyk de Vries, 1993; Walker et al., 1993; Wehrmann et al., 2006; Kutterolf et al., 2007). Kutterolf et al. (2007) suggested that the San Antonio Tephra, with a

volume of >14 km³ may have led to the formation of a 6 km by 11 km, northwest trending caldera (Fig. 1). Several explosive eruptions are documented since the formation of the caldera that might have contributed to its subsidence, including the large-volume phreatomagmatic deposits of the Masaya Tuff, erupted <2 ka (Pérez and Freundt, 2006; Kutterolf et al., 2007). These eruptions were large volume (12–18 km³ dense rock equivalent) and resulted in widespread tephra fallout and pyroclastic flows (Williams, 1983a).

A prominent caldera rim was formed during these events. The rim is up to 400 m high on the west and northwest side of the caldera. It is ~200 m high above Laguna Masaya (Fig. 1) on the eastern side of the caldera. On the south side, the caldera rim has less relief and is partially buried by post-caldera lava flows and tephra from post-caldera vents to the SW. The caldera rim is subdued, or buried, on the north side of the caldera and its exact position is inferred. The caldera walls, where exposed, consist of thin aa-pahoehoe lava

Table 1

Summary of TEM soundings collected in Masaya caldera. Map coordinates are given in UTM Zone 16N WGS84. Depth to water table is estimated from two separate inversion algorithms. For relative locations within the caldera see Fig. 2

Sounding #	Easting	Northing	Loop size (m)	Land surface elevation (masl)	Depth to water (m) Einvt 6	Depth to water (m) EMVision
1	0592483	1326524	100	3322 80	51.3	59.1
2	0591925	1327235	100	280	141.5	141
3	0591987	1327689	100	278	172	173.1
4	0590327	1325187	100	482	143	132.1
5	0591718	1324863	100	569	218.7	234
6	0591970	1325700	100	478	243.1	255.3
7	0595709	1325804	40	162	46	46.3
8	0594825	1326305	100	196	78.8	88.8
9	0594284	1326177	100	228	111.9	122.6
10	0594861	1322311	40	155	–	–
11	0595063	1323995	40	176	48.1	51.2
12	0594507	1324507	100	206	70.3	84.1
13	0594096	1325103	100	228	88.5	98.8
14	0599840	1327928	100	310	164.4	169.5
15	0592399	1328274	100	285	175	179.2
16	0593029	1328183	100	288	169.2	173
17	0592132	1328845	100	305	152.1	158.5
18	0590050	1324351	100	422	244.8	241.5
19	0599466	1324338	100	390	243.6	235.4
20	0599067	1325056	100	336	219	216.1
21	0590572	1328827	100	311	171.8	177.4
22	0590072	1328554	100	311	176.2	179.5
23	0591384	1329045	100	322	165.4	172.3
24	0594511	1321208	40	162	7.8	18.6
25	0595648	1325386	40	120	5.9	21
26	0590421	1324668	100	522	294.8	285.4
27	0590325	1325698	100	459	183.5	195.1
28	0590157	1325997	100	420	221	244.6
29	0590423	1326424	100	358	202.3	208.7
30	0590093	1327779	100	322	185	193.1

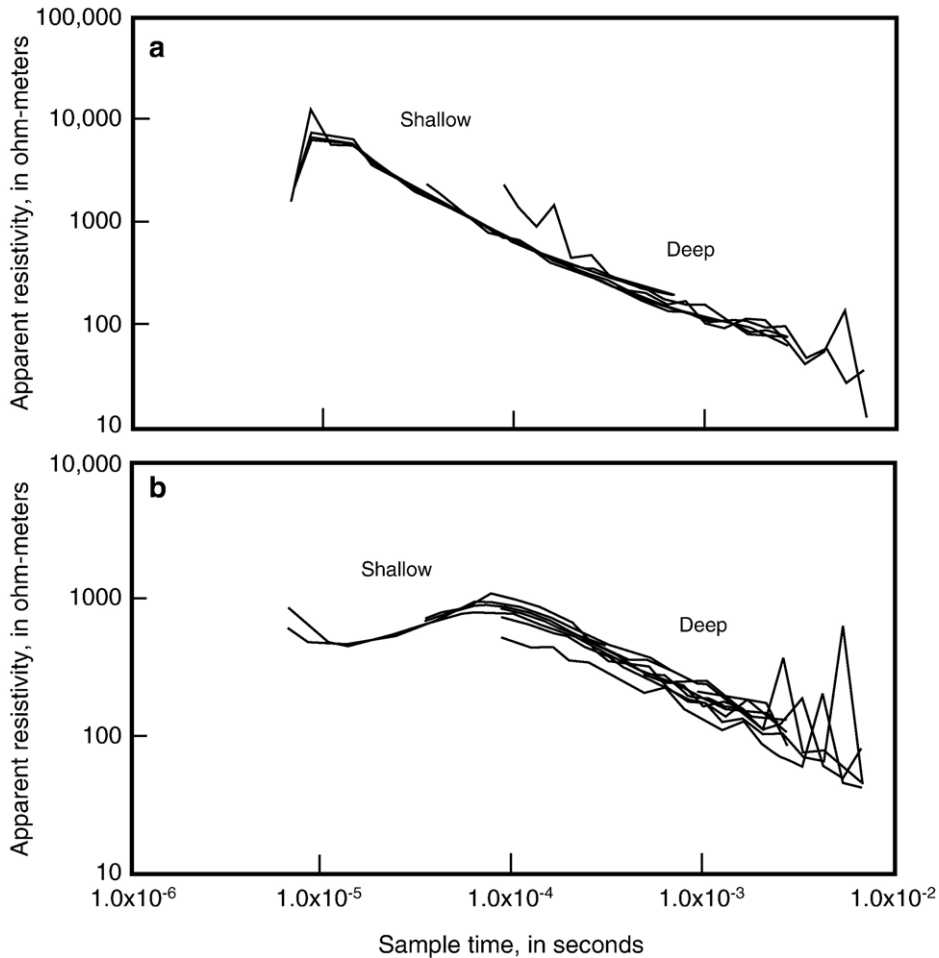


Fig. 3. Examples of apparent resistivity curves used for preliminary interpretation of TEM soundings at Masaya caldera. (a) Most apparent resistivity curves from TEM soundings at Masaya caldera show a highly resistive upper layer underlain at depth by one or more conductive layers (TEM sounding 3 shown). On the southwestern side of the historically active vents, near the older Piedra Quemada lava flow, (b) the uppermost layer has a slight conductive zone, probably produced by either alteration of the Piedra Quemada flow or the influence of the less-resistive, underlying San Judas Formation tephra deposits (TEM sounding 18 shown). Multiple curves are shown for repeated measurements at the same stations.

flows and pyroclastic fall and flow deposits (Williams, 1983b). The total amplitude of vertical offset across these caldera-bounding faults is not clear from geologic outcrops or other data. Slip may have been very large if the caldera formed predominantly by foundering during evacuation of a large magma chamber (Williams, 1983a). Post-caldera activity included the eruption of lava flows from caldera-bounding faults mapped by Williams (1983b) on the south and north flanks of the caldera (Walker et al., 1993). Thus lithologic and hydrologic properties are likely to change abruptly across the caldera boundary.

Volcanic activity persisted after these caldera-forming eruptions. The floor of the caldera slopes gently to the east (Fig. 2) and is armored by thin aa-pahoehoe basaltic lava flows, largely erupted from a group of vents within the

caldera. These vents form a ~ 5 -km-long, W- to NW-trending, semi-circular group of low volcanic cones. Pit craters at the summit of these cones, including Masaya, Santiago, Nindiri, and San Pedro pit craters, were the locus of historical eruptions in 1670 and 1772 that formed 10–15 km-long lava flows (Rymer et al., 1998). The elevation of the crater rims along this chain of pit craters varies from 500 to 635 masl, and heights of these crater rims are ~ 140 –275 m above the surrounding caldera floor (Fig. 1). Each of these pit craters is 400–1000 m in diameter and has very steep walls, with crater depth varying between 200–300 m.

Today, active degassing is almost entirely limited to Santiago pit crater and a lava lake is occasionally visible in vents through the floor of the crater. Based on time-series of gravity observations on and about this cone complex,

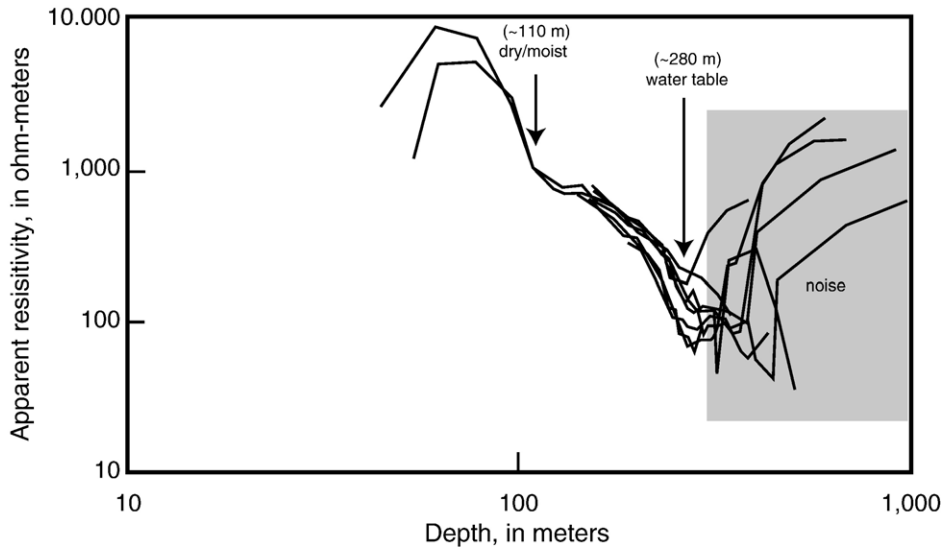


Fig. 4. Graphical example of analytical solution used at TEM 26 that transforms apparent resistivity values to resistivity with approximate depth values (Meju, 1998).

Rymer et al. (1998) and Williams-Jones et al. (2003) concluded that much of the pit-crater alignment is underlain by a network of gas-rich, vesiculated magma extending from approximately 200 masl (the elevation of the floor of the Santiago pit crater) to ~200 mbsl. This shallow crystallizing magma is the source of persistent degassing from Santiago crater since 1852 (Rymer et al., 1998) and infrequent small explosions. Rymer et al. (1998) and Williams-Jones et al. (2003) attribute these small explosions to purely magmatic processes. They suggest that the explosions result from blockages in the degassing vent just below the surface. Pressure builds until a small explosion clears the vent. There also are anecdotal reports that these explosions occur preferentially during

the rainy season and may be associated with recharge of the groundwater system. However, explosions have not occurred in response to exceptional recharge events, such as that associated with hurricane Mitch in 1998.

Although occasional explosions at Santiago pit crater may conceivably be influenced by interaction with meteoric water, this large and complex magmatic system otherwise appears to be in equilibrium with the groundwater system. On the NE flank of Masaya volcano, within the caldera, a fault and fracture zone hosts outflow of water vapor and CO₂ at moderate temperatures (40–70 °C), indicating that groundwater interacts with magmatic heat, and perhaps volcanic gases, well outside the pit crater system (Lewicki et al.,

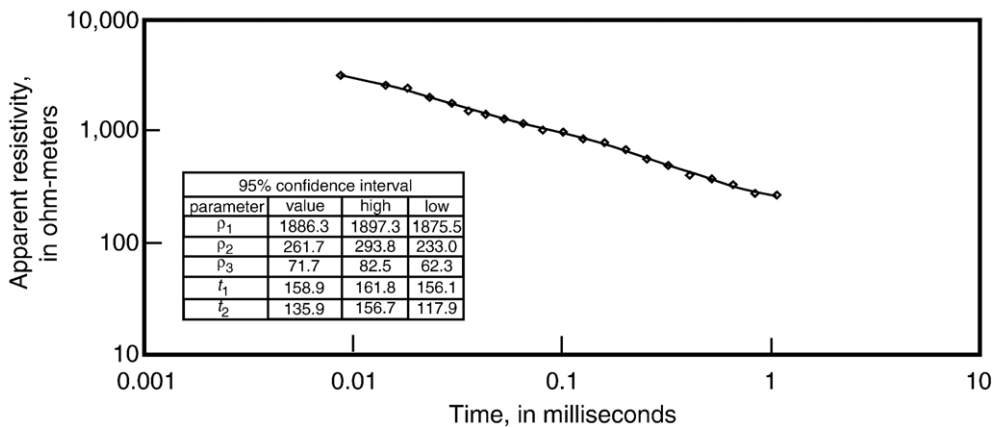


Fig. 5. Inverse modeling results for TEM 26 using the program by Sandberg (1988). The apparent resistivity definition used is the late-stage solution from Eq. (1). The squares are observed values and the solid line is the model fit.

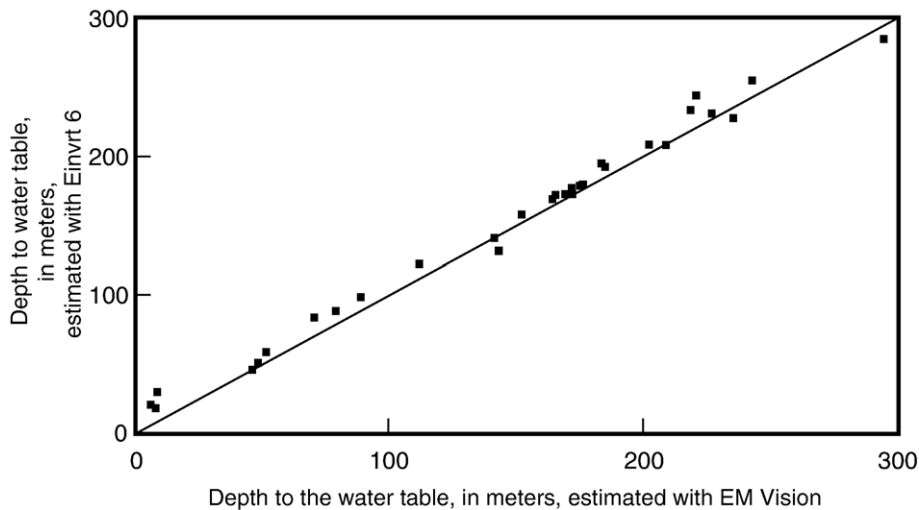


Fig. 6. Comparison of the two inversion programs show consistent results with the EINVRT 6 program modeling the water table an average of 8.2% shallower than the EM Vision models. See Table 1.

2003, 2004). Nevertheless, other than along this one fracture zone, there is no evidence that an extensive hydrothermal system is present within caldera outside the active vent complex.

Data from a regional ground water flow model developed in 1993 by the Instituto Nicaraguense de Acueductos y Alcantarillados (ENECAL) and the Japanese International Cooperation Agency (JICA) indicate that regional groundwater levels vary from ~190 masl south of the caldera to ~130 masl north of the caldera (Fig. 1) (ENECAL and JICA, 1993). Rainfall is high in the caldera (~1600 mm/yr), yet no persistent surface water flow occurs in or around it. Regional evapotranspiration rates are high (~1100 mm/yr). No borehole data exist within the caldera itself, and prior to this study the only indication of water levels in the caldera was the level of Lake Masaya (Fig. 1), which is monitored monthly by ENACAL. Lake levels during this investigation were ~119 masl. This lake level is below the regional groundwater table (Fig. 1), suggesting that the lake is not perched, but represents the level of the groundwater table in the caldera.

3. Mapping groundwater with the transient electromagnetic method

The transient electromagnetic method (McNeill, 1982, Kaufmann and Keller, 1983, Fitterman and Stewart, 1986) has been used extensively in geophysical groundwater exploration and, along with other electrical resistivity methods, has been used to investigate shallow hydrothermal systems on volcanic edifices (Sakkas

et al., 2002). In recent geoelectrical studies of volcanic systems, TEM has provided high-resolution data in the near surface (<1 km), and has been used to identify hydrothermal fluid circulation and aquifer systems. The correlation of borehole data and TEM sounding depths for low resistivity regions on Kilauea volcano, Hawaii, Mt. Somma-Vesuvius, Italy, Piton de la Fournaise volcano, Réunion, and Newberry volcano, Oregon, have shown the effectiveness of this method (Fitterman et al., 1988; Kaahikaua, 1993; Lenat et al., 2000; Manzella et al., 2004). Nevertheless, care is required to assure that estimates of depth to the water table are not affected by clay alteration in the stratigraphic section or perched water zones. At Masaya caldera, the volcanic geology and hydrologic conditions create a situation in which deposits with high electrical resistivities host a water table at depths >100 m. Porous, saturated lava flows and scoria of the caldera floor offer an excellent electrical contrast with the overlying, dry basaltic rocks. Deeply exposed walls in the active vent show little evidence of clay alteration in the edifice. Also, most of the caldera that is close to land surface is at ambient temperature, and Lake Masaya provides an excellent water level for calibration of nearby TEM soundings.

4. TEM soundings

Multiple soundings of different frequencies were made at 30 sites throughout the caldera (Table 1, Fig. 2). TEM data were collected using a Geonics Limited Protem 47 Digital Time Domain EM system and high-frequency receiver coil (McNeill, 1980). We used the

central-loop sounding-mode configuration, because it has been used extensively and effectively in other groundwater studies (Kaufmann and Keller, 1983; Fitterman and Stewart, 1986). Data were collected at 20 logarithmically spaced time gates following transmitter turnoff. Transmitter loops were square, 40 m on a side near Laguna Masaya and 100 m throughout the remainder of the caldera, where the anticipated depth to the water table was greater. Data were collected at three different base frequencies: 30, 75, and 285 Hz, with the receiver gain set to minimize environmental noise, yet generate a survey signal appropriate for the given geologic terrain without distortion to the measurement. Output current on the Protom 47 transmitter was set from 1 Amp (A) to 3 A when using the smaller 40 m loops and at 3 A for 100 m loops. Multiple soundings and signal stacking were performed at each site to maximize the signal-to-noise ratio and to evaluate reproducibility of the sounding.

The TEM sites are situated throughout the caldera, with an emphasis on the historically active crater region and its flanks. Several sites were adjacent to Laguna Masaya for verification of depth-to-water-table estimates. The remaining TEM sites are in the northern and northeastern sections of the caldera where there is little change in vertical relief. No soundings were made in the southeastern and extreme western portions of the caldera due to the difficulty of the terrain and lack of access, but these regions are similar in elevation and slope to the northern and eastern areas.

5. Data processing

All TEM data were transformed to apparent resistivity for preliminary interpretation, data quality assessment, and to assist in initial parameters for layered-earth inverse models (Fig. 3a and b). The data were transformed using the technique of Sandberg (1988),

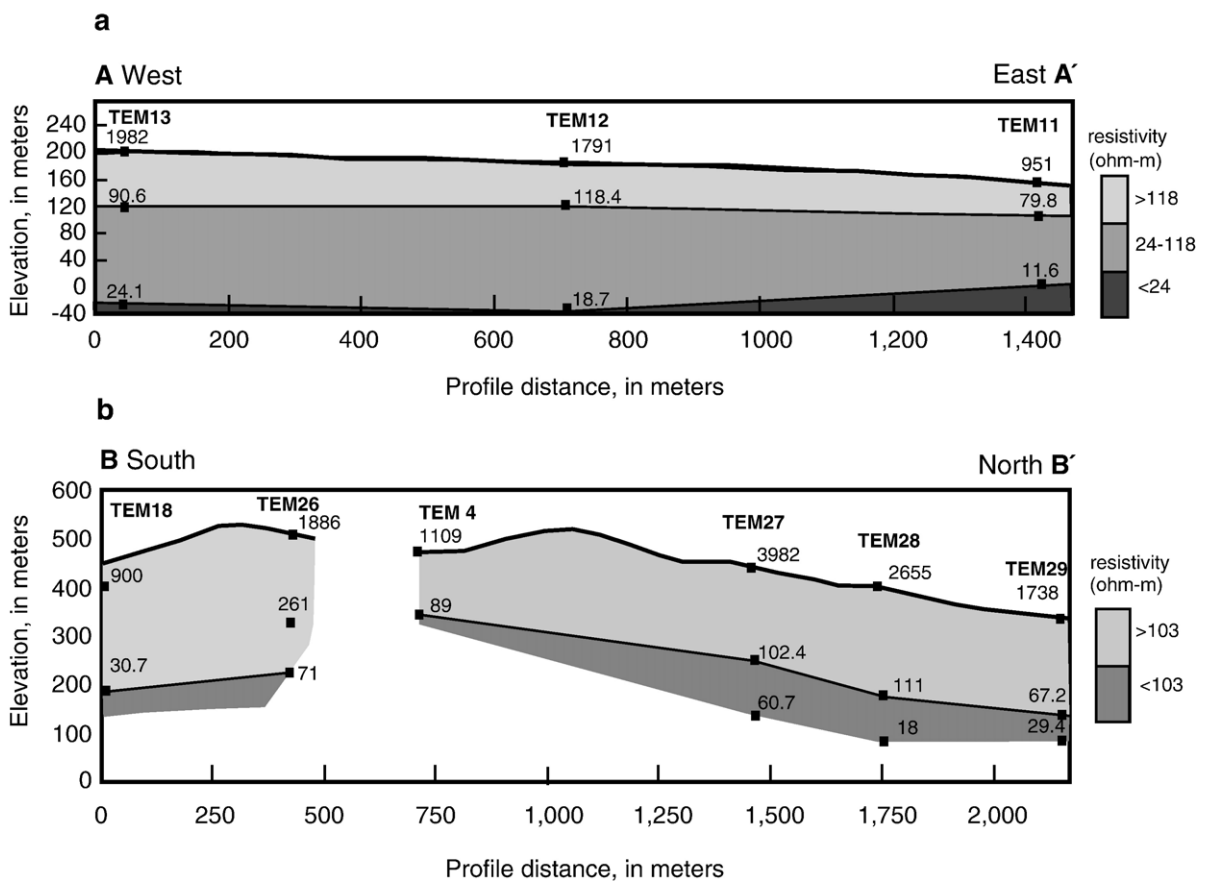


Fig. 7. Apparent resistivity cross-sections along profiles (a) A–A' in the eastern caldera near Laguna Masaya and (b) B–B' near the active vent region. Apparent resistivity values are shown based on the Meju (1998) solution. The transition from light to medium gray represents the estimated elevation of the water table, based on inverse modeling results (Table 1).

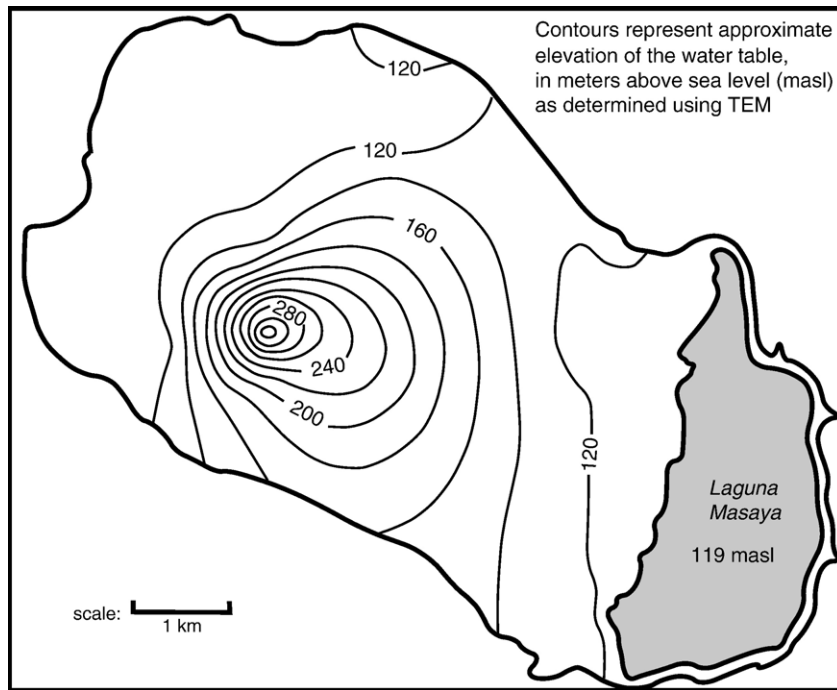


Fig. 8. Contour map of the estimated groundwater table at Masaya caldera from TEM measurements. The map is intended to show the general pattern of water-table elevation, and was generated from a statistically kriged data field that, at some points, varies from the measured data by several meters.

which accounts for the finite transmitter-turnoff ramp. For large sample times (t), and/or high resistivities (ρ), this apparent resistivity definition asymptotes to the so-called late-stage approximation calculated by:

$$\rho_a^{\text{late}} = \frac{\alpha^{4/3} A_R^{2/3} \mu^{5/3}}{20^{2/3} \pi^{1/3} t^{5/3} Z^{2/3}} \quad (1)$$

where a is the equivalent circular transmitter-loop radius, A_R is the effective area of the receiver coil, μ is the magnetic permeability (the free-space value, $\mu_0 = 4\pi \times 10^{-7}$, was used), t is the time since transmitter current turnoff, and Z is the mutual impedance (voltage in the receiver coil divided by the current in the transmitter loop).

Most apparent resistivity versus time curves from TEM soundings at Masaya caldera show a highly resistive upper layer underlain at depth by one or more conductive layers (Fig. 3a). However, on the southwestern side of the historically active vents, near the older Piedra Quamada lava flow, the uppermost layer has a slight conductive zone. This zone is probably produced either by alteration of the Piedra Quamada lava flow or by the influence of the less resistive underlying San Judas Formation tephra deposits described by Williams (1983a) (Fig. 3b).

The TEM data were modeled using two independent methods to estimate resistivity as a function of depth.

The first method utilizes an analytical solution that transforms apparent resistivity values to resistivity with approximate depth values (Meju, 1998). The pattern of high and low resistivity layers is much more obvious in apparent resistivity versus depth curves (Fig. 4) calculated using the Meju (1998) solution.

The results are used to produce contoured resistivity cross sections and to compare modeling methods. The second method uses two commercially available programs (EM Vision from Encom and EINVRT 6 from Geophysical Solutions) that employ non-linear, least-squares regression algorithms to adjust layered-earth parameters, such as layer thickness and resistivity values, through an iterative process to minimize error (Sandberg, 1988). The EINVRT 6 program utilizes a Marquardt-type method that results in an undamped 95% confidence level (Hohmann and Raiche, 1988; Sandberg, 1988, 1993; Fig. 5). The method used by EM Vision relies on the GRENDL algorithm for 1D inversion and outputs a 68% confidence level. All models are 1-D interpretations and were run with the fewest number of layers that give a reasonable fit to field data.

6. Discussion of TEM

The two inversion programs show consistent results and comparison of the inversion models to the analytical

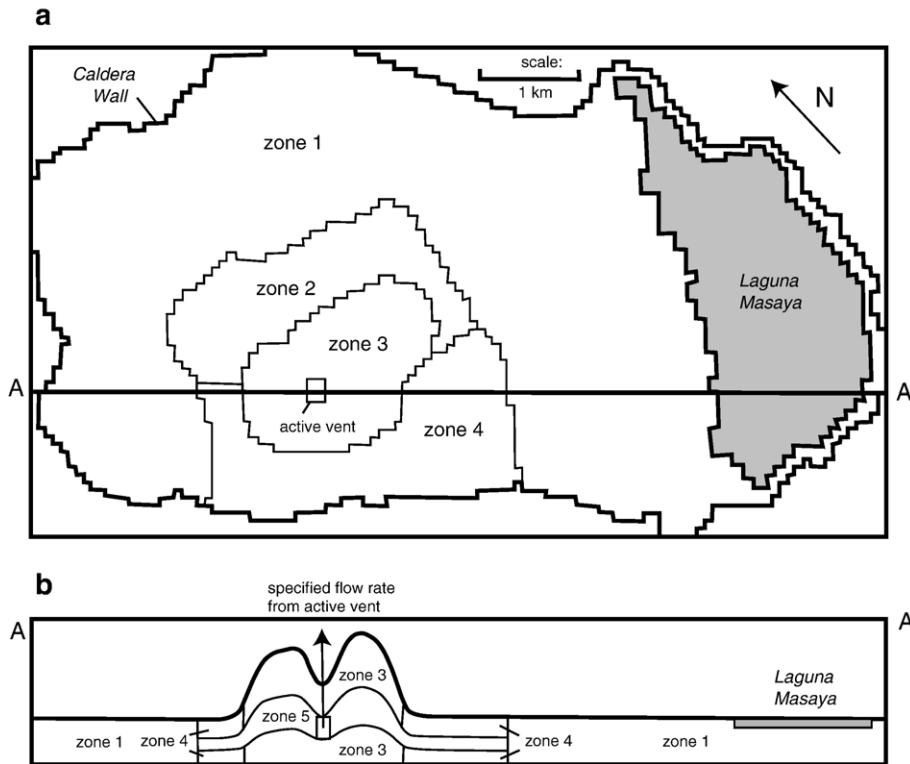


Fig. 9. The three-dimensional groundwater flow model of Masaya caldera, showing the (a) horizontal, and (b) vertical distributions of the hydraulic-parameter zones. See Table 2.

Meju solution shows similar results for most TEM soundings. EINVRT 6 modeled the water table as being an average of 8.2% shallower than the EM Vision models (Fig. 6). This translates to a mean difference of 7.8 m between the two models. Due to the greater constraint on the data by the EINVRT 6 program with its calculated undamped 95% confidence intervals, we believe it provides a better statistical model of the system. The overall accuracy of the TEM method varies across the survey area. Near the lake the lake, comparison of TEM model results and lake levels indicates an accuracy of within 2 m (e.g., sounding #7, Table 1). In contrast, near the active Santiago vents the water table is much deeper, the electrical structure is more complex, and the accuracy is likely no better than tens of meters (e.g., Sounding #4, Table 1).

Models of the TEM data indicate an overlying highly resistive layer throughout the caldera that is underlain by one or more conductive layers. The depth to the conductive layers increases with distance from Laguna Masaya towards the topographically high volcanic vents. The large apparent resistivity contrast in the subsurface is interpreted to be the interface between dry overlying basalt and the underlying saturated zone

below the water table. This contrast is shown by the shallow conductive layer (<118 ohm-m) detected by TEM soundings 7 and 11 near Laguna Masaya (Fig. 2). This conductive layer coincides with the elevation of the nearby lake at ~119 masl, and is assumed to be the top of the water table (Fig. 7). Under this assumption, the top of the conductive layer throughout the caldera is interpreted to be the top of the saturated zone. The water table in the caldera is nearly flat except in the higher vent regions in the central and southern portions of the caldera. Across the elevated vent region, the water table or conductive zone is a subdued replica of the topography. The resistivity cross section there (Fig. 7b) shows a large variation in the water table between TEM 26 and TEM 4 along profile B–B', near the active Santiago vent. The apparently shallower water table and lower resistivities found at TEM 4 may be due a vapor-dominated zone near the active vent, although the 1-D inversion cannot fully capture the 3-D complexity of the near-vent region.

The TEM-based water table in the caldera is very different from the regional water levels projected from the JICA groundwater model. In that model, the regional ground water flow system is not affected by the presence

Table 2
Hydraulic parameters calibrated for the groundwater model of the caldera. For zone locations see Fig. 9

Zone number	Hydraulic conductivity (m/day)	Intrinsic permeability (m ²)	Transmissivity (m ² /s)
1	650	7.7×10^{-10}	9×10^{-1}
2	.03	3.5×10^{-14}	4×10^{-5} to 6×10^{-5}
3	.0054	6.4×10^{-15}	7×10^{-6} to 3×10^{-5}
4	.023	2.7×10^{-14}	4×10^{-5} to 6×10^{-5}
5	45	5.3×10^{-11}	2×10^{-2}

of Masaya caldera (Fig. 1). Our study indicates head values (Fig. 8) as much as 60 m lower than those proposed from the JICA data (Fig. 1) on the western, southern, and eastern boundaries of the caldera and slightly lower values (10–20 m), on the northern side of the caldera, where the caldera rim has no surface expression. The inference of a large change in head values across the caldera boundaries suggests that the caldera walls are hydrologic barriers, so that the caldera is hydrologically isolated from the surrounding region.

Masaya caldera differs from most other basaltic shield volcanoes in having a large volume of water vapor emissions under quiescent conditions (Burton et al., 2000). A substantial proportion of the water vapor may be of meteoric origin. If the caldera is hydrologically isolated, evapotranspiration in the caldera and degassing of meteoric water from the active vents must balance recharge to the system. Consequently, changes in volcanic activity, such as increased vaporization of groundwater due to heating, should be reflected in changes in the level of the water table. Our assessment of the elevation of the water table at Masaya caldera is a first step in looking at the shallow hydrologic system. A second step is to quantify the flux of water through the system. We use numerical simulation of groundwater flow in the caldera to compare estimates of fluxes and water-table elevations.

7. Groundwater model formulation

The groundwater system in Masaya caldera is highly complex. The volcanic edifice is highly heterogeneous and contains fault and fracture zones that have a visible impact on water and vapor transport. High temperatures in the active crater create a steam-dominated zone and affect fluid density in the surrounding regions. To incorporate all of these effects into one model would require a multiphase code that can incorporate complex three-dimensional

heterogeneous terrains. The objective of this study was to gain an understanding of the flow system at a more basic level; such an objective can be met using a simpler, constant-density, single-phase modeling approach. To accomplish this, the USGS code MODFLOW2000 (Harbaugh et al., 2000) was used to construct a three-dimensional flow model of the caldera.

A finite-difference grid was constructed of 10 layers, 64 rows, and 113 columns, and was aligned along the long axis of the crater to optimize the percentage of active grid cells (Fig. 9). Each grid cell is about 100 m in each horizontal dimension. In the vertical dimension the cells are about 12 m thick beneath most of caldera, but are thicker beneath the edifice by an amount that is proportional to the entire model thickness (Fig. 9b). Information on lithologies and their hydraulic characteristics at depth inside the crater are nonexistent, so the bottom of the model was arbitrarily chosen to be at sea level (a simplification that is consistent with the rest of this modeling scope). As MODFLOW2000 does not consider variable saturation in the soil zone, the top of such a model is usually placed either at the land surface or at the approximate level of the water table. The former option is accompanied by a variable saturation condition in the top layer(s), whereas the latter assumes a confined condition. The latter option was chosen for this study to avoid the nonlinear convergence problems that sometimes occur with cells that become dry during modeling in MODFLOW2000. Lake Masaya was treated as a constant head boundary, and the caldera

Table 3
Estimates of water fluxes at Masaya Caldera

Flux type	Source of data	In kg/s	In m ³ /year per m ² of land surface	In m ³ /year per m ² of lake
Rainfall	Measured		1.6	1.6
Evapotranspiration from land surface	Rainfall minus recharge, and consistent with Maraux et al. (1998)		1.1	
Recharge	Steam discharge plus groundwater flow to			
Laguna Masaya	665	0.5		
Evaporation from Laguna Masaya	Eagleman (1967)	795		2.4
Groundwater flow into Laguna Masaya	Evaporation at lake minus rainfall at lake	265	0.2	0.8
Steam discharge at active vent	Burton et al. (2000)	400	0.3	

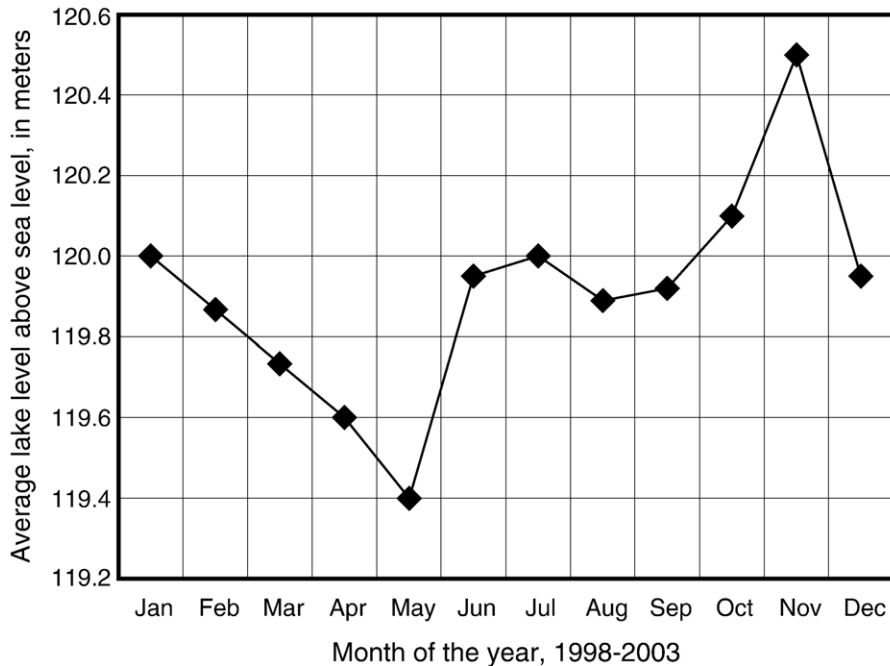


Fig. 10. Mean monthly water levels of Laguna Masaya for the years 1998–2003.

boundary (lateral boundary) was assigned a general-head boundary condition. This condition allows the leakage of water through the caldera wall to be adjusted to create a match between water levels inside and outside the caldera. As there is actually a great disparity between these two sets of water levels, the leakance was set low enough that the caldera walls act as a virtual no-flow boundary. In reality, a small amount of groundwater may cross the caldera walls, especially at the eastern end, around Laguna Masaya.

The caldera was divided into five hydraulic conductivity zones to represent the different lithologic hydraulic conditions that exist throughout the caldera (Fig. 9). No subsurface borehole data is available, so these zones were chosen to represent the overall geology as observed from the surface and the behavior of the groundwater system near the active vent. The largest zone (zone 1) is dominated by lava flows in the northern and eastern caldera. The flanks of the edifice were divided into two sections (zones 2 and 4), and the main central edifice was defined separately (zone 3). The land surface within the active craters was represented by drain cells (not shown). This was done to represent the fact that groundwater does not accumulate as a lake in the craters, but is drawn down by evapotranspiration and thermal vaporization. Simulation results indicated that a fifth zone was required within the edifice to allow groundwater to

flow toward the active vent without depleting water higher in the edifice. The parameter estimation process in MODFLOW2000 was used to adjust the values of hydraulic conductivity for the zones to best fit the water levels estimated by the TEM surveys. The values that were converged upon are listed in Table 2. Also listed are the transmissivities, which may be a more useful result, given the lack of data on vertical lithologic variability and depth of the active flow system. The value for zone 1 contains the greatest uncertainty, as the very flat water table indicates a relatively high but poorly constrained value of hydraulic conductivity.

8. Groundwater flux estimates

Water levels alone cannot produce unique values of hydraulic conductivity through inverse modeling of a groundwater flow system. Flux measurements were also required to constrain the model parameters. Flux estimates were obtained from three sources: (1) rainfall and evapotranspiration, (2) groundwater inflows to Lake Masaya, and (3) steam discharge from the active vent. The values of these fluxes are summarized in Table 3.

Recharge was prescribed across the surface of the caldera as a fraction of the high rainfall in the region (1.6 m per year). Because no data exist for groundwater

recharge fluxes in the caldera, a value of 0.5 m/yr was selected based in part on studies of humid volcanoes at Kilauea (Takasaki, 1993; Ingebritsen and Scholl, 1993) and the Cascades Range (Ingebritsen et al., 1992; Manga, 1997). This value also was close to a value that was calculated by balancing the groundwater budget. In reality, recharge in the caldera is spatially variable and likely to be a function of vegetation cover, with recharge in vegetated areas likely less than nonvegetated areas because of transpiration. The open areas are often bare lava flows, with large openings at the land surface that would allow for quick and efficient infiltration during

rainfall events. The evapotranspiration rate (Table 3) is not an input for this model, but can be calculated as the rainfall rate minus the recharge rate. For this case the value of 1.1 m/year is similar to other values reported in Nicaragua (e.g., Maraux et al., 1998).

Direct water flux measurements at Laguna Masaya were not available, but some estimates could be made using other flux components. Evaporation from the lake surface can be estimated from climatic variables (e.g., Eagleman, 1967). Surface water inflow to the lake is minor, so that a long-term steady-state balance requires that rainfall plus groundwater inflow equal evaporation.

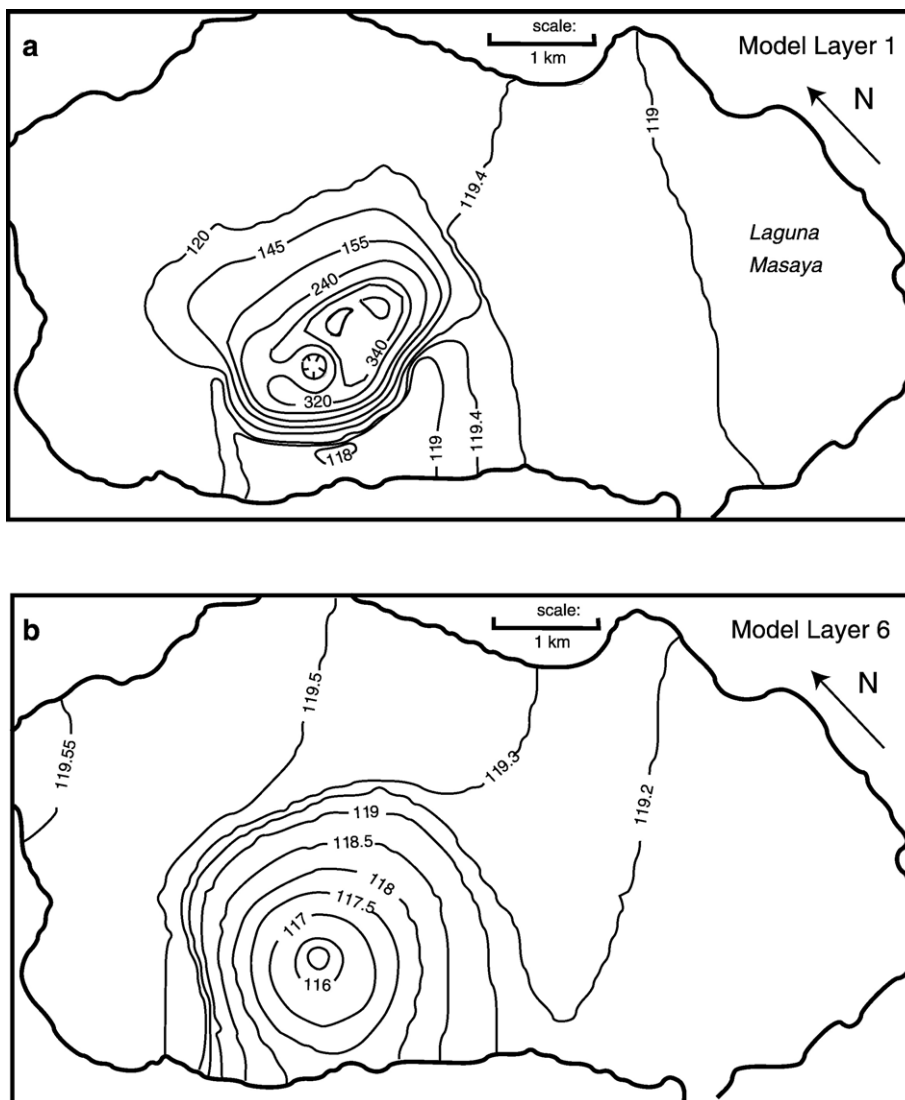


Fig. 11. Simulated groundwater levels (hydraulic heads) in (a) layer 1, and (b) layer 6 of the ground water model. Layer 1 is the shallowest and its head values represent the water table. Layer 6 is deeper and includes the high permeable zone 5 (Fig. 9) that transmits water toward the active vent. The distribution of hydraulic heads in layers 1 and 6 reflect our best estimates of the hydraulic conditions within the caldera.

Thus a groundwater inflow rate could be estimated based on the other two major fluxes. A completely closed lake would cause build-up of dissolved salts in the lake over time and a saline Laguna Masaya would result. As this is not the case, there is likely some small amount of groundwater discharge to the regional flow system that we cannot quantify at this time. Seasonal changes in the lake level show a steady decline during the months of January through April (Fig. 10). Given that precipitation during this dry season is nearly zero, mass balance requires that this rate of lake level decline (1.6 m/year) be nearly equivalent to the precipitation rate, as is the case.

The final water flux component within the caldera is that of the steam exiting at the active vent in Santiago Crater. This flux was estimated to be approximately 400 kg/s by earlier investigations (Burton et al., 2000). Although some of this vapor may have a magmatic origin, its magnitude suggests a high likelihood that most of it is of meteoric origin. Thus we used this value to define a point discharge of groundwater in the model. The point discharge was represented by a well at the active crater discharging from zone 5 (Fig. 9) at a rate of 400 kg/s. This is a large fraction of the water budget, roughly 60% of recharge within the caldera (Table 3). The remaining 40% is assumed to discharge to Laguna Masaya.

9. Simulation results

The final calibrated water levels and gradients are similar to those estimated by the TEM measurements (compare Figs. 8 and 11a). The simulated elevation of the water table in layer 1 (Fig. 11a) reflects the calibration and fit to the TEM data. The water-level gradient is very flat in the outer reaches of the caldera underlain by lava flows. Water levels beneath the flanks of the edifice begin to increase in value, and then increase substantially beneath the central edifice. During the model calibration process, the water level at the active vent was not allowed to drop below the approximate elevation of the bottom of Santiago Crater (about 100 m amsl). Fig. 11b shows the same hydrologic model for a deeper model layer. In order to maintain sufficient flow toward the active vent, and maintain discharge from the vent of approximately 400 kg/s, the hydraulic conductivity of zone 5 (Fig. 9) had to be increased to roughly 45 m/day. As a result of the point discharge, a cone of depression develops within zone 5 that extends outward across the entire edifice (Fig. 11b). On the basis of this hydraulic head distribution, it can be inferred that much of the rainfall that recharges the edifice may discharge out the main vent, whereas

rainfall that recharges the outer regions of the caldera may discharge to Laguna Masaya.

10. Discussion of groundwater at Masaya

In terms of electrical structure, the caldera consists of a highly resistive layer that is underlain by one or more conductive layers. The top of the conductive layers is interpreted to be the water table and is expressed as a subdued replica of the topography in the higher vent regions, decreasing to a level that coincides with the elevation of Laguna Masaya in the topographically lower areas of the caldera. There is a large (up to 60 m) decrease in head values across the caldera boundaries, suggesting that the caldera is hydraulically isolated from the surrounding region. Offset across caldera-bounding faults may be responsible for abrupt changes in transmissivity. Alternatively, post-caldera lavas are reported to have erupted along caldera-bounding faults (Walker et al., 1993). Dike injection associated with these lavas may have reduced transmissivity.

Increase in the depth to the water table near the active vent region of Santiago crater is consistent with vaporization of groundwater due to heating, previously suggested to be a substantial component of the gas emissions at Masaya caldera. The conversion of 400 kg/s of liquid water at ambient temperatures to steam requires a very large heat input (1000 MW) that would be originating from beneath the edifice and driving convection of flow towards the edifice at depth.

Numerical simulations of groundwater flow in the caldera suggest markedly different hydraulic transmissivities in different sections of the caldera. The outer caldera, outside of the main edifice, is characterized by basalt flows that have very high transmissivity. In order to transmit groundwater to the active vent at a rate that is equal to the steam discharge, a highly transmissive layer must also exist somewhere at depth beneath the main edifice. The groundwater model does not further constrain the geologic nature of this transmissive layer and it may consist of either fractured lavas or intra-caldera pyroclastic units. In contrast, the rocks comprising most of the main edifice must have relatively low transmissive properties, as low values are required to maintain the high water table observed there. The low values are consistent with values of young altered volcanic rocks in Hawaii and Oregon (Ingebritsen et al., 1992; Ingebritsen and Scholl, 1993). Alternatively, the low values could be explained by a high water table under perched conditions, with the calibrated transmissivities for the main edifice representing values at partial saturation.

Both the estimated water table elevations and the water budget fluxes for the caldera have substantial uncertainty. The fluxes (except for rainfall) have uncertainties that we estimate to be as large as 25%. Further, the multiphase nature of the system around the active vents could not be adequately represented in this study.

The highly connected and transmissive nature of the subsurface at Masaya suggests that groundwater levels may fluctuate in response to magmatic activity. Installation of observation wells in the caldera could facilitate a refined study of the groundwater system and help observe and detect volcanic activity. The successful conjunctive use of TEM and numerical simulation at Masaya also suggests that a similar approach may be useful at other volcanoes.

Acknowledgments

This research project at Masaya was made possible due to financial support provided in part by the USGS Volcano Hazards Program. We especially appreciate the assistance of the entire staffs from the Parque Nacional Volcán Masaya, ENECAL, and especially W. Strauch, Eduardo Mayorga, José Manuel Traña, and Enoc Castillo from INETER. We would also like to thank Pedro Pérez and Félix Henrique for their invaluable help while working at Masaya caldera, and Mark Stewart from the University of South Florida for discussions on the hydrogeologic system. We thank Editor Margaret Mangan, two anonymous reviewers, Steve Ingebritsen, and Shaul Hurwitz for their help in improving this manuscript.

References

- Burton, M.R., Oppenheimer, C., Horrocks, L.A., Francis, P.W., 2000. Remote sensing of CO₂ and H₂O emission rates from Masaya volcano, Nicaragua. *Geology* 28 (10), 915–918.
- Connor, C., Hill, B., LaFemina, P., Navarro, M., Conway, M., 1996. Soil ²²²Rn pulse during the initial phase of the June–August 1995 eruption of Cerro Negro, Nicaragua. *Journal of Volcanology and Geothermal Research* 73, 119–127.
- Delaney, P.T., 1982. Rapid intrusion of magma into wet rock: groundwater flow due to pore pressure increases. *Journal of Geophysical Research* 87, 7739–7756.
- DeMets, C., 2001. A new estimate for present-day Cocos-Caribbean plate motion: implications for slip along Central American volcanic arc. *Geophysical Research Letters* 28 (21), 4043–4046.
- Eagleman, J.R., 1967. Pan evaporation, potential evaporation and actual evaporation. *Journal of Applied Meteorology* 6, 482–488.
- ENACAL and JICA, 1993. Hydrogeological map of Managua, Nicaragua, Instituto Nicaraguense de Acueductos y Alcantarillados and Japanese International Cooperation Agency, Managua, Nicaragua, Scale 1:50,000.
- Fitterman, D.V., Stewart, M.T., 1986. Transient electromagnetic sounding for groundwater. *Geophysics* 51 (4), 995–1005.
- Fitterman, D.V., Stanley, W.D., Bisdorf, R.J., 1988. Electrical structure of Newberry volcano, Oregon. *Journal of Geophysical Research* 93 (B9), 10119–10134.
- Goff, F., Janik, C.J., 2000. Geothermal systems. In: Sigurdsson, H. (Ed.), *Encyclopedia of Volcanology*. Academic Press, pp. 817–855.
- Harbaugh, A.W., Banta, E.R., Hill, M.C., McDonald, M.G., 2000. MODFLOW-2000, the U. S. Geological Survey modular groundwater model-user guide to modularization concepts and the ground-water flow process. U. S. Geological Survey Open-File Report, vol. 00-92.
- Hayba, D.O., Ingebritsen, S.E., 1997. Multiphase groundwater flow near cooling plutons. *Journal of Geophysical Research* 102, 12235–12252.
- Hohmann, G.W., Raiche, A.P., 1988. Inversion of controlled-source electromagnetic data. In: Nabighian, M.N. (Ed.), *Electromagnetic Methods in Applied Geophysics, Volume 1: Investigations in Geophysics*, vol. 3. Society of Exploration Geophysicists, Tulsa, OK, pp. 469–503.
- Hurwitz, S., Kipp, K.L., Ingebritsen, S.E., Reid, M.E., 2003. Groundwater flow, heat transport, and water table position within volcanic edifices: implications for volcanic processes in the Cascade Range. *Journal of Geophysical Research* 108. doi:10.1029/2003JB002565.
- Ingebritsen, S.E., Scholl, M.A., 1993. The hydrogeology of Kilauea Volcano. *Geothermics* 22, 255–270.
- Ingebritsen, S.E., Sherrod, D.R., Mariner, R.H., 1992. Rates and patterns of groundwater flow in the Cascade Range volcanic arc, and the effect on subsurface temperatures. *Journal of Geophysical Research* 97, 4599–4627.
- Ingebritsen, S.E., Sanford, W.E., Neuzil, C.E., 2006. *Groundwater in Geologic Processes*. Cambridge University Press, Cambridge.
- Kauahikaua, J., 1993. Geophysical characteristics of the hydrothermal systems of Kilauea volcano, Hawaii. *Geothermics* 22 (4), 271–299.
- Kaufmann, A.A., Keller, G.V., 1983. *Frequency and Transient Soundings*. Elsevier, Amsterdam.
- Kutterolf, S., Freundt, A., Pérez, W., Wehrman, H., Schminke, H.-U., 2007. Late Pleistocene to Holocene temporal succession and magnitudes of highly-explosive volcanic eruptions in west-central Nicaragua. *Journal of Volcanology and Geothermal Research* 163, 55–82.
- La Femina, P.C., Dixon, T.H., Strauch, W., 2002. Bookshelf faulting in Nicaragua. *Geology* 30 (8), 751–754.
- Lénat, J.F., Fitterman, D., Jackson, D.B., Labazuy, P., 2000. Goelectrical structure of the central zone of Piton de la Fournaise volcano (Réunion). *Bulletin of Volcanology* 62, 75–89.
- Lewicki, J., Connor, C., St-Armand, K., Stix, J., Spinner, W., 2003. Self-potential, soil CO₂ flux, and temperature on Masaya volcano, Nicaragua. *Geophysical Research Letters* 30 (15), 1817–1821.
- Lewicki, J.L., Hilley, G.E., Connor, C.B., 2004. The scaling relationship between self-potential and fluid flow on Masaya volcano, Nicaragua. In: Wanty, R.B., Seal II, R.R. (Eds.), *Water–Rock Interaction*. Taylor and Francis Group, London. ISBN: 90 5809 6416, pp. 153–156.
- Manga, M., 1997. A model for discharge in spring-dominated streams and implications for the transmissivity and recharge of Quaternary volcanics in the Oregon Cascades. *Water Resources Research* 33, 1813–1822.
- Manzella, A., Volpi, G., Zaja, A., Meju, M., 2004. Combined TEM–MT investigations of shallow-depth resistivity structure of Mt Somma-Vesuvius. *Journal of Volcanology and Geothermal Research* 131, 19–32.
- Maraux, F., Lafolle, F., Bruckler, L., 1998. Comparison between mechanistic and functional models for estimating soil water

- balance. Deterministic and stochastic approaches. *Agricultural Water Management* 38 (1), 1–20.
- McNeill, J.D., 1980. Applications of Transient Electromagnetic Techniques, Technical Note TN-7. Geonics Ltd, Mississauga Canada. 15 pp.
- McNeill, J.D., 1982. Use of electromagnetic methods for groundwater studies. In: Ward, S.H. (Ed.), *Geotechnical and Environmental Geophysics, Volume II: Environmental and Groundwater, Investigations in Geophysics No. 5*. Society of Exploration Geophysicists, Tulsa, OK, pp. 191–218.
- Meju, M.A., 1998. A simple method of transient electromagnetic data analysis. *Geophysics* 63 (2), 405–410.
- Morrissey, M., Zimanowski, B., Wohletz, K., Buettner, R., 2000. Phreatomagmatic fragmentation. *Encyclopedia of Volcanology*. Academic Press, pp. 431–445.
- Newhall, C.G., Albano, S.E., Matsumoto, N., Sandoval, T., 2001. Roles of groundwater in volcanic unrest. *Journal of the Geological Society of the Philippines* 56, 69–84.
- Pérez, W., Freundt, A., 2006. The youngest highly explosive basaltic eruptions from Masaya Caldera (Nicaragua): stratigraphy and hazard assessment. In: Rose, W.I., Bluth, G.J.S., Carr, M.J., Ewert, J., Patino, L.C., Vallance, J.W. (Eds.), *Volcanic Hazards in Central America*. Geological Society of America Special Paper, 412, pp. 189–207.
- Rymer, H., van Wyk de Vries, B., Stix, J., William-Jones, G., 1998. Pit crater structure and processes governing persistent activity at Masaya volcano, Nicaragua. *Bulletin of Volcanology* 59, 345–355.
- Sandberg, S.K., 1988. Inverse Modeling Software for Resistivity, Induced Polarization (IP), and Transient Electromagnetic (TEM, TDEM) Soundings. Geophysical Solutions, Inc., Albuquerque, New Mexico.
- Sandberg, S.K., 1993. Examples of resolution improvement in geoelectrical soundings applied to groundwater investigations. *Geophysical Prospecting* 41, 207–227.
- Sakkas, V., Meju, M.A., Khan, M.A., Haak, V., Simpson, F., 2002. Magnetotelluric images of the crustal structure of Chyulu Hills volcanic field, Kenya. *Tectonophysics* 346, 169–185.
- Shibata, T., Akita, F., 2001. Precursory changes in well water level prior to the March 2000 eruption of Usu volcano, Japan. *Geophysical Research Letters* 28 (9), 1799–1802.
- Sparks, S., 2003. Forecasting volcanic eruptions. *Earth and Planetary Science Letters* 210, 1–15.
- Takasaki, K.J., 1993. Ground water in Kilauea Volcano and adjacent areas of Mauna Loa, Island of Hawaii. U. S. Geological Survey Open-File Report, vol. 93-82.
- Van Wyk de Vries, B., 1993. Tectonics and Magma Evolution of Nicaragua Volcanic Systems, Ph.D. Thesis, Open University, Milton Keynes, UK (unpublished).
- Walker, J.A., Williams, S.N., Kalamarides, R.I., Feigenson, M.D., 1993. Shallow open-system evolution of basaltic magma beneath a subduction zone volcano: the Masaya Caldera Complex, Nicaragua. *Journal of Volcanology and Geothermal Research* 56, 379–400.
- Wehrmann, H., Bonadonna, C., Freundt, A., Houghton, B.F., Kutterolf, S., 2006. Fontana Tephra: a basaltic Plinian eruption in Nicaragua. In: Rose, W.I., Bluth, G.J.S., Carr, M.J., Ewert, J., Patino, L.C., Vallance, J.W. (Eds.), *Volcanic Hazards in Central America*. Geological Society of America Special Paper, 412, pp. 209–223.
- William-Jones, G., Rymer, H., Rothery, D.A., 2003. Gravity changes and passive SO₂ degassing at the Masaya caldera complex, Nicaragua. *Journal of Volcanology and Geothermal Research* 123, 137–160.
- Williams, S.N., 1983a. Plinian airfall deposits of basaltic composition. *Geology* 11, 211–214.
- Williams, S.N., 1983b. Geology and eruptive mechanisms of Masaya Caldera Complex, Nicaragua, PhD thesis, Dartmouth College, Hanover, NH, (unpubl.)